Electron momentum distributions and photoelectron spectra of atoms driven by intense spatially inhomogeneous field

M. F. Ciappina[1,2], J. A. Pérez-Hernández[3], T. Shaaran[1], L. Roso [3], and M. Lewenstein[1,4]

[1]*ICFO-Institut de Ciències Fotòniques, Mediterranean Technology Park, 08860 Castelldefels (Barcelona), Spain*
[2]*Department of Physics, Auburn University, Auburn, Alabama 36849, USA*
[3]*Centro de Láseres Pulsados, CLPU, Parque Científico, 37185 Villamayor, Salamanca, Spain and*
[4]*ICREA-Institució Catalana de Recerca i Estudis Avançats, Lluis Companys 23, 08010 Barcelona, Spain*

We use three dimensional time-dependent Schrödinger equation (3D–TDSE) to calculate angular electron momentum distributions and photoelectron spectra of atoms driven by spatially inhomogeneous fields. An example for such inhomogeneous fields is the locally enhanced field induced by resonant plasmons, appearing at surfaces of metallic nanoparticles, nanotips and gold bow-tie shape nanostructures. Our studies show that the inhomogeneity of the laser electric field plays an important role in the above threshold ionization process in the tunneling regime, causing significant modifications to the electron momentum distributions and photoelectron spectra, while its effects in the multiphoton regime appear to be negligible. Indeed, through tunneling ATI process, one can obtain higher energy electrons as well as high degree of asymmetry in the momentum space map. In this study we consider near infrared laser fields with intensities in the mid- 10^{14} W/cm^2 range and we use linear approximation to describe their spatial dependence. We show that in this case it is possible to drive electrons with energies in the near-keV regime. Furthermore, we study how the carrier envelope phase influences the emission of ATI photoelectrons for few-cycle pulses. Our quantum mechanical calculations are fully supported by their classical counterparts.

PACS numbers: 42.65.Ky,78.67.Bf, 32.80.Rm

I. INTRODUCTION

The process known as above-threshold ionization (ATI), in which an atom or molecule absorbs more photons than the minimum number required to single ionize it, has been a subject of intensive studies during the last decades (see e.g. [1] and references therein). The first experimental realization was made at the end of the seventies [2] and since then there has been a truly amazing progress in understanding of the non-perturbative nature of ATI. The recent advances in laser technology made possible to routinely generate laser pulses with few cycles of duration, which allows control of the atomic and molecular processes in their natural time scales, i.e. in the range of (sub)-femto to attoseconds. In addition, these short laser sources find an extensive range of applications in basic science, such as controlling molecular motions and chemical reactions [3, 4]. Furthermore, the few-cycles pulses provide the fundamental pillar in the generation of high-order harmonics and the creation of isolated extreme ultraviolet (XUV) pulses [5, 6].

The appearance of COLTRIMS experiments (see e.g. [7] and references therein) offered an unprecedented possibility of performing stringent tests on the different theoretical approaches. On one side, this is because the imaging of the vectorial momentum distributions of the reaction fragments are easily accessible, while on the other they are particularly sensitive to various details of the theory. COLTRIMS were primarily developed for the study of few-body dynamics induced by particle impact, i.e. electrons and ions, but the extension to scrutinize and tackle laser-induced processes was natural (see e.g [8–10]). Among the features which were theoretically

analyzed was the complex emission pattern present in the two-dimensional momentum plane, parallel and perpendicular to the laser polarization axis, of the laser-ionized electron distributions near threshold [11]. It was also investigated how these patterns evolve as the laser-matter process change from the multiphoton to the tunneling regimes [10].

The main difference between a few-cycle pulse and a multicycle one is the strong dependence of the laser electric field on the so-called Carrier Envelope Phase (CEP) [12, 13]. The electric field in a few-cycle pulse can be characterized by its duration and by the CEP. The influence of CEP has been experimentally observed in high-harmonic generation (HHG) [14], the emission direction of electrons from atoms [15], and in the yield of nonsequential double ionization [16]. In order to have a better control of the system on an attosecond temporal scale it is, therefore, important to find reliable and direct schemes to measure the absolute phase of few-cycle pulses.

The investigation of ATI generated by few-cycle driving laser pulses plays a key role in the CEP characterization due to the sensitivity of the energy and angle-resolved photoelectron spectra to the value of the laser electric field absolute phase [17, 18]. Consequently, the behavior of the laser-ionized electrons renders the ATI phenomenon a very valuable tool for laser pulse characterization. To determine the CEP of a few-cycle laser pulse, it is essential to record the difference between the yield of electrons ionized for different emission angles. Through this technique one can analysis the so-called backward-forward asymmetry in order to obtain the absolute CEP [19]. Furthermore, it appears that the high

energy region of the photoelectron spectra is most sensitive to the absolute CEP and consequently electrons with large kinetic energy are needed in order to describe it [1, 20].

Recent experiments using a combination of plasmonic nanostructures and rare gases have demonstrated that the harmonic cutoff of the gases could be extended further than in conventional situations by using the field, locally enhanced due to the coupling of a laser pulse with a nanosystems [21, 22]. In such nanosystems, due to the strong confinement of the plasmonics spots and the distortion of the electric field by the surface plasmons, the locally enhanced field is not spatially homogeneous in the region, where the electron dynamics take place. One should note, however, that the outcome of the experiments of Ref. [21], in which a combination of gold bowtie nanostructure and argon gas for generation HHG was used, has been recently under intense scrutiny [23, 24]. In addition, recently, instead of atoms or molecules in gas phase solid state nanostructures have been employed as a target to study the photoelectron emission by few intense laser pulses [25, 26]. This laser driven phenomenon, called Above Threshold Photoemission (ATP), has received special attention due to the novelty of the involved physics and potential applications. In ATP process, the emitted electrons have energy far beyond the usual cutoff for noble gases (see e.g. [26–31]). Furthermore, the photoelectrons emitted from these nanosources are sensitive to the CEP, and consequently this fact plays an important role in the angle and energy resolved photoelectron spectra [25, 26, 32, 33].

From theoretical point of view, the fundamental assumption behind strong field phenomena, that the laser field is spatially homogeneous in the region where the electron dynamics takes place [34, 35], is not any more valid for the locally enhanced plasmonic field. Indeed, in such system the driven electric field, and consequently the Lorentz force the electron feels, will also depend on position. Up to now, there have been very few studies investigating the strong field phenomena in such spatially inhomogeneous fields [36–42]. All of these studies have demonstrated that the spatial dependency of the field strongly modifies the laser-driven phenomena that appear in such circumstances.

For homogeneous driving field, up to know, different numerical and analytical approaches have been employed to calculate the ATI (see e.g. [1, 43–47] and references therein). In this article, we extend the studies of our previous paper [40] by applying the numerical solution of the time-dependent Schrödinger Equation (TDSE) in three dimensions to calculate the angular electron momentum distributions and photoelectron spectra of ATI driven by spatially inhomogeneous fields, considering both tunneling and multiphoton regimes. The spatial dependence of the field is considered to be linear. We mainly focus on studying ATI of hydrogen atoms, but our scheme, within the single active electron approximation, can be directly applied to any complex atom. We demonstrate how the inhomogeneity of the field modifies both the two electron momentum distributions and the photoelectron spectra; we examine also the influence of the CEP parameter. Furthermore, our quantum mechanical results are compared with classical calculations of the kinetic energy of the electron.

This article is organized as follows. In the next section, we present our theoretical approach to model ATI produced by spatially nonhomogeneous fields, with main emphasis on the extraction of the electron angular momentum distributions starting from the TDSE outcomes. Subsequently, in Sec. III, we apply our method to compute the electron momentum distributions and energy-resolved photoelectron spectra of hydrogen atom using few-cycle laser pulses for both homogeneous and inhomogeneous fields, considering tunneling and multiphoton regimes. Furthermore, we solve the classical equations of motion of an electron in an oscillating inhomogeneous electric field to support our quantum mechanical method. Finally, in Sec. IV, we conclude our contributions with a short summary and outlook.

II. THEORETICAL APPROACH

To study the properties of the ATI phenomenon driven by spatial nonhomogeneous fields, we solve the three dimensional Time Dependent Schrödinger Equation (3D-TDSE) in the length gauge. The electron momentum distribution and energy-resolved photoelectron spectra of an atom are calculated from the time propagated electronic wave function.

Our calculations are based on spherical harmonics expansion, Y_l^m, considering only the $m = 0$ terms due to the cylindrical symmetry of the problem. The Crank-Nicholson method, which is based on a splitting of the time-evolution operator that preserves the norm of the wave function, is used as the numerical technique. We consider the field to be linearly polarized along the z axis and the variation of the electric field is linear with respect to the position. As a result, the coupling $V_l(\mathbf{r}, t)$ between the atomic system and the electromagnetic radiation reads

$$V_l(\mathbf{r}, t) = \int^{\mathbf{r}} d\mathbf{r}' \cdot \mathbf{E}(\mathbf{r}', t) = E_0 z (1 + \beta z) f(t) \sin(\omega t + \phi),$$
(1)

where E_0, ω and ϕ are the laser electric field amplitude, the central frequency and characterizes the carrier envelope phase (CEP), respectively. The parameter β defines the 'strength' of the inhomogeneity and has units of inverse length (see also [36–38]). For modeling the short laser pulses in Eq. (1), we use a sin-squared envelope $f(t)$ of the form

$$f(t) = \sin^2\left(\frac{\omega t}{2n_p}\right),$$
(2)

where n_p is the total number of optical cycles. As a result, the total duration of the laser pulse will be $T_p = n_p \tau$

where $\tau = 2\pi/\omega$ is the laser period. We also assume that before switch on of the laser ($t = -\infty$) the target atom (hydrogen) is in its ground state ($1s$), whose analytic form can be found in standard textbooks. Within the single active electron approximation, however, our numerical scheme is tunable to treat any complex atom by choosing the adequate effective (Hartree-Fock) potential, and finding the ground state by the means of numerical diagonalization.

The ATI spectrum is calculated using the time dependent wave function method developed by Schafer and Kulander (see [48] for more details). As a preliminary test, for ensuring the consistence of our numerical simulations, we have checked out our calculations with the results previously obtained in Ref. [48]. The comparison confirms the high degree of accuracy of our calculations as shown in Fig. 1.
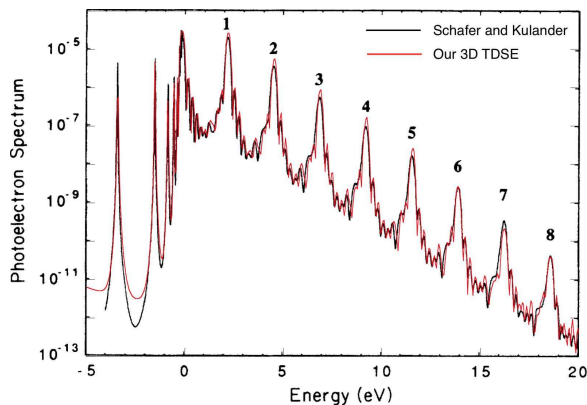
FIG. 1. (Color online) Photoelectron spectrum resulting from our 3D TDSE simulations (in red) and superimposed (in black) with the ATI results calculated by Schafer and Kulander in Ref. [48]. The laser wavelength is $\lambda = 532$ nm and the intensity is $I = 2 \times 10^{13}$ W/cm^2 (see Fig.1 in [48] for more details. The superimposed plot has been extracted from Fig. 1 of this cited reference.

For calculating the energy-resolved photoelectron spectra $P(E)$ and two-dimensional electron distributions $\mathcal{H}(p, \theta)$ we use the window function approach developed by Schafer [48, 49]. This tool has been widely used, both to calculate angle-resolved and energy-resolved photoelectron spectra [50], and it represents a step forward with respect to the usual projection methods.

III. RESULTS

In this section, we calculate both energy-resolved photoelectron spectra $P(E)$ and two-dimensional electron momentum distributions in order to investigate the influence of the inhomogeneities of the field and the sensitivity of these two measurable quantities to the different laser parameters, especially to the carrier envelope phase (CEP). The investigations are carried out for both the tunneling regime, for which the Keldysh parameters is

$\gamma \lesssim 1$ ($\gamma = \sqrt{I_p/2U_p}$, where $U_p = I/4\omega^2$ is the ponderomotive energy and I_p the ionization potential), and multiphoton regime, for which the Keldysh parameters is $\gamma >> 1$. Furthermore, we confirm how in the tunneling regime the CEP, joint with the spatial nonhomogeneities, modify in a particular way both the energy-resolved photoelectron spectra and the two-dimensional electron momentum distributions as we have shown in our previous contribution [40]. On the other hand, we show that in the multiphoton regime ($\gamma >> 1$), the spatial nonhomogeneous character of the laser electric field hardly affects the analyzed quantities. We also want to point out, however, that the frontier between the tunnel and multiphoton regimes appears to be a controversial and diffuse issue [51, 52].

A. Tunneling regime

We commence by investigating the tunneling regime. For this case, we employ a four-cycle (total duration 10 fs) sin-squared laser pulse with wavelength $\lambda = 800$ nm and two different intensities, namely $I = 1.140 \times 10^{14}$ W/cm^2 and $I = 5.0544 \times 10^{14}$ W/cm^2. These two intensities give values for the laser electric field of $E_0 = 0.057$ a.u. and $E_0 = 0.12$ a.u., respectively. For all the cases we chose four different values for the parameter that characterizes the inhomogeneity strength, namely, $\beta = 0$ (homogeneous case), 0.002, 0.003 and 0.005. In addition we also vary the carrier envelope phase ϕ in Eq. (1), taking $\phi = 0$, $\phi = \pi/2$, $\phi = \pi$ and $\phi = 3\pi/2$. For all the above mentioned cases, we calculate the the energy-resolved photoelectron spectra. The results are shown in Figures 2 and 3 for $I = 1.140 \times 10^{14}$ W/cm^2 ($\gamma = 1$) and $I = 5.0544 \times 10^{14}$ W/cm^2 ($\gamma = 0.475$), respectively.
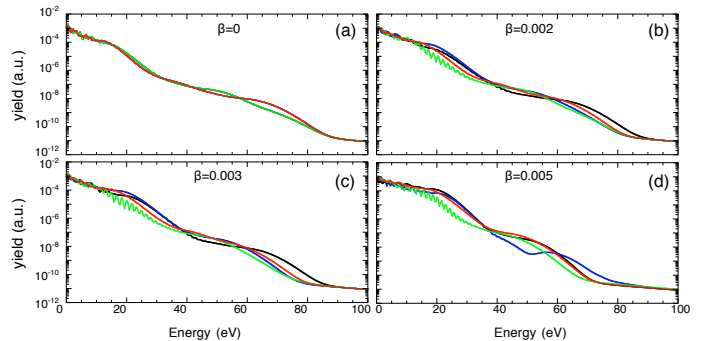

FIG. 2. (Color online) Energy-resolved photoelectron spectra $P(E)$ calculated using the 3D-TDSE for an hydrogen atom ($I_p = -0.5$ a.u.). The laser parameters are $I = 1.140 \times 10^{14}$ W/cm^2 ($E_0 = 0.057$ a.u.) and $\lambda = 800$ nm. We have used a sin-squared shaped pulse with a total duration of four optical cycles (10 fs). (a) $\beta = 0$ (homogeneous case), (b) $\beta = 0.002$, (c) $\beta = 0.003$ and (d) $\beta = 0.005$. In all the panels, black line: $\phi = 0$; blue line $\phi = \pi/2$; green line: $\phi = \pi$ and red line: $\phi = 3\pi/2$.

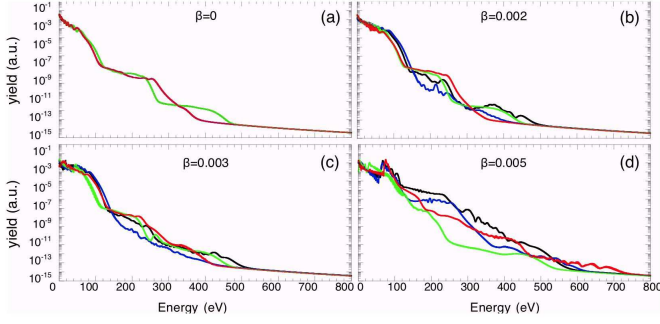For the homogeneous case, the spectra exhibits the

FIG. 3. (Color online) Idem Fig. 2 but for a laser intensity $I = 5.404 \times 10^{14}$ W/cm^2 ($E_0 = 0.12$ a.u.).

usual distinct behavior, namely, the $2U_p$ cutoff (≈ 13.6 eV in Fig. 2(a) and ≈ 57.4 eV in Fig. 3(a)) and the $10U_p$ cutoff (≈ 68 eV in Fig. 2(a) and ≈ 300 eV in Fig. 3(a)). The former cutoff corresponds to those electrons that, once ionized, never return to the atomic core (the so-called *direct* electrons), while the latter one corresponds to the electrons that, once ionized, return to the core and elastically rescatter (the so-called *rescattered* electrons). Classically, it is a well established arguments that the maximum kinetic energies E_k of the direct and the rescattered electrons are $E^d_{max} = 2U_p$ and $E^r_{max} = 10U_p$, respectively (see below for more details). In a quantum mechanical approach, however, it is possible to find electrons with energies beyond the $10Up$ cutoff, although their yield drops several orders of magnitude depending strongly on the atomic species studied [1].
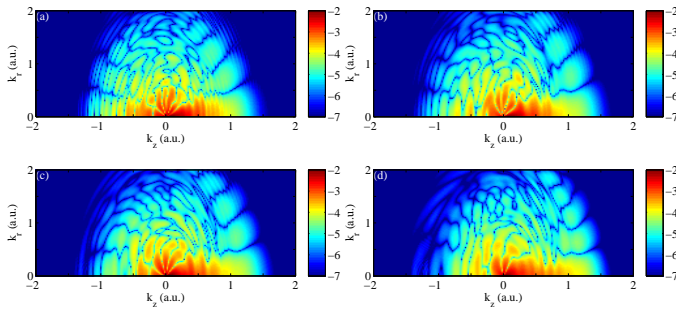
FIG. 4. (Color online) Two-dimensional electron momentum distributions (logarithmic scale) in cylindrical coordinates (k_z, k_r) using the exact 3D-TDSE calculation for an hydrogen atom. The laser parameters are $I = 1.140 \times 10^{14}$ W/cm^2 ($E_0 = 0.057$ a.u.) and $\lambda = 800$ nm. We have used a sin-squared shaped pulse with a total duration of four optical cycles (10 fs) with $\phi = 0$. (a) $\beta = 0$ (homogeneous case), (b) $\beta = 0.002$, (c) $\beta = 0.003$ and (d) $\beta = 0.005$.

Experimentally speaking, both the direct and rescattered electrons contribute to the energy-resolved photo-

electron spectra. It means for tackling this problem both physical mechanisms should be included in theoretical model. In that sense, the 3D-TDSE, which can be considered as an exact approach to the ATI problem for atoms in the single active electron approximation, is the adequate tool to predict the $P(E)$ in the whole range of electron energies. On the other hand, the most energetic electrons, i.e., those with kinetic energies $E_k \gg 2U_p$, are commonly used to characterize the CEP of few-cycle pulses. Consequently, a correct description of the electron rescattering mechanism is needed.
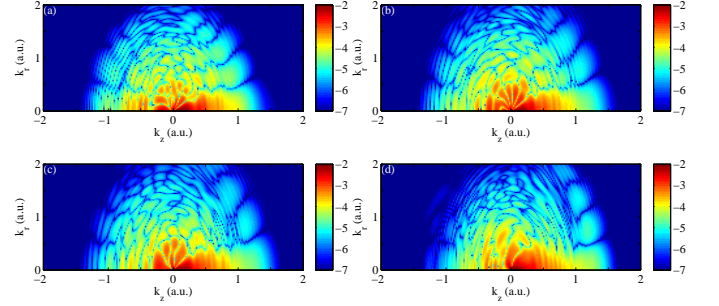

FIG. 5. (Color online) Idem Fig. 4 but for $\phi = \pi/2$

For the spatially nonhomogeneous cases, the positions of the direct and the rescattered electron cutoffs are extended towards larger energies. For the rescattered electrons, this extension is very noticeable. In fact for $\beta = 0.005$ with $E_0 = 0.12$ a.u., it reaches values close to ≈ 700 eV [Fig. 3(d)] against the ≈ 300 eV shown by the homogeneous case. Another new feature present for all the nonhomogeneous cases is the strong sensitivity of the $P(E)$ to the carrier envelope phase (CEP). This behavior can be clearly noticed by comparing the panels (a) of Figs. 2 and 3 (i.e. the homogeneous case) with the rest of the plots. It is clear that for the homogeneous case only two curves are present, due to the fact that the $P(E)$ for $\phi = 0$ and ($\phi = \pi/2$) are identical to $\phi = \pi$ and ($\phi = 3\pi/2$), respectively. On the other hand, for all the nonhomogeneous cases it is possible to clearly distinguish the 4 cases, i.e. $\phi = 0$, $\phi = \pi/2$, $\phi = \pi$ and $\phi = 3\pi/2$. Indeed, this particular characteristic of the $P(E)$ for nonhomogeneous fields could make them a new and better CEP characterization tool.

It should be noted, however, that other well-known and established CEP characterization tools, such as, for instance, the forward-backward asymmetry or two-dimensional electron momentum distributions should complement the $P(E)$ measurements [1]. Furthermore, the utilization of nonhomogeneous fields would open the avenue for the production of high-energy electrons, reaching the keV regime, if a reliable control of the spatial and temporal shape of the laser electric field is attained. Investigations in such direction has already started (see e.g. [29] and references therein).

A deep analysis of the electron distributions for atomic ionization produced by an external laser field can be per-
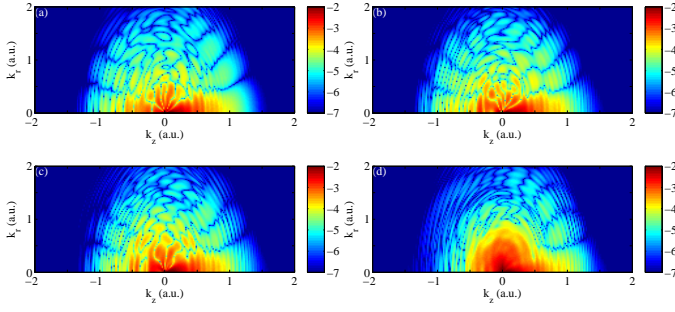
FIG. 6. (Color online) Idem Fig. 4 but for $\phi = \pi$

formed in terms of the two-dimensional electron momentum distribution. The exact solution of the three dimensional Schrödinger equation (3D-TDSE) provide us with an excellent tool to analyze in detail how the two competing fields, namely the laser electric field and the Coulomb potential, modify the electron wavepacket of the released electron. In Figs. 4-7 we calculate two-dimensional electron momentum distribution for a laser field with an intensity of $I = 1.140 \times 10^{14}$ W/cm^2 ($E_0 = 0.057$ a.u), $\lambda = 800$ nm and different values of the the β parameter: panel (a) $\beta = 0$ (homogeneous case); panel (b) $\beta = 0.002$; panel (c) $\beta = 0.003$ and panel (d) $\beta = 0.005$. We employ a few-cycle laser pulse with 4 total cycles (10 fs) and various values of the carrier envelope phase (CEP) parameter ϕ. Figs. 4-7 show the cases with $\phi = 0$, $\phi = \pi/2$, $\phi = \pi$ and $\phi = 3\pi/2$, respectively.
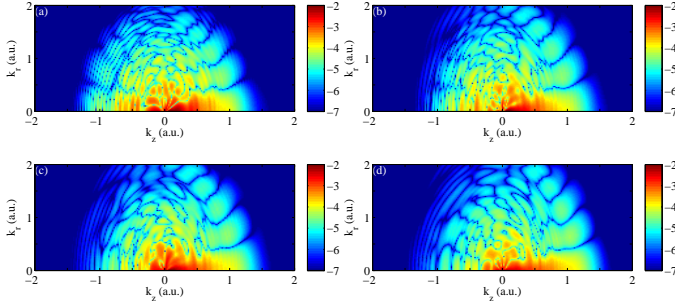
FIG. 7. (Color online) Idem Fig. 4 but for $\phi = 3\pi/2$

Here, we concentrate our analysis on the low energy region of the distributions in order to study how the inhomogeneities of the laser electric field affect the angular electron yield. This region shows the usual *bouquet*-type structures (see [11] for details) with noticeable modifications for the nonhomogeneous cases.

Furthermore, the low-energy electrons appear to be strongly influenced by the spatial inhomogeneity of the laser electric field (see panels (b)-(d) of Figs. 4-7). We also can observe how the *bouquet* structures present in the homogeneous case *disappear* for particular values of ϕ (see e.g. Fig.6(d)).

In order to complete our investigations, we calculate two-dimensional electron momentum distributions by in-
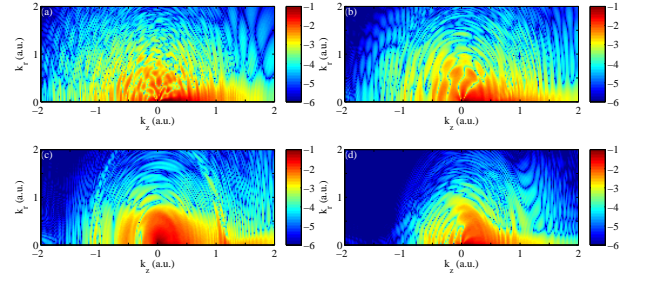

FIG. 8. (Color online) Two-dimensional electron momentum distributions (logarithmic scale) in cylindrical coordinates (k_z, k_r) using the exact 3D-TDSE calculation for an hydrogen atom. The laser parameters are $I = 5.0544 \times 10^{14}$ W/cm^2 ($E_0 = 0.12$ a.u.) and $\lambda = 800$ nm. We have used a sin-squared shaped pulse with a total duration of four optical cycles (10 fs) with $\phi = 0$. (a) $\beta = 0$ (homogeneous case), (b) $\beta = 0.002$, (c) $\beta = 0.003$ and (d) $\beta = 0.005$.

creasing the laser field intensity to $I = 5.0544 \times 10^{14}$ W/cm^2 ($E_0 = 0.12$ a.u). The results are depicted in Figs. 8-10 for $\phi = 0$, $\phi = \pi/2$, $\phi = \pi$ and $\phi = 3\pi/2$, respectively. Here, panel (a), (b), (c) and (d) represent the cases with $\beta = 0$ (homogeneous case), $\beta = 0.002$, $\beta = 0.003$ and $\beta = 0.005$, respectively.
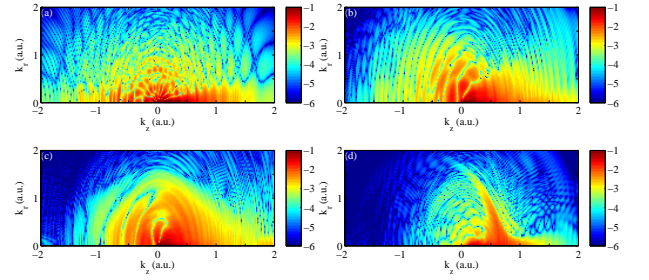

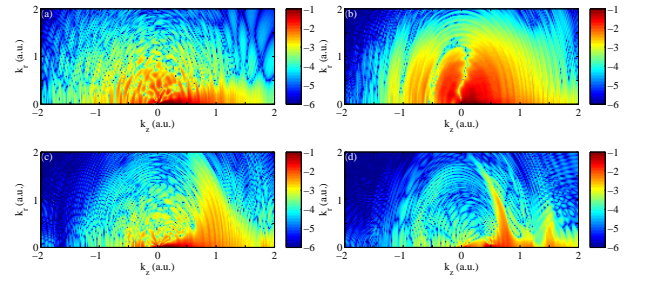FIG. 9. (Color online) Idem Fig. 8 but for $\phi = \pi/2$

FIG. 10. (Color online) Idem Fig. 8 but for $\phi = \pi$

Following the trend observed in the previous studied case, we see strong modifications produced by the spatial inhomogeneities in both the angular and low-energy structures. Here, the modification seems to be even more pronounced. For instance, the yield for electrons with $k_z < -1$ a.u. for $\phi = 0$ (Fig. 8(a)) and $\phi = \pi/2$ (Fig. 9(a)) drops several orders of magnitude. The sig-

nificant drop of the yield of the electron emission between $k_z < -1$ a.u and $k_z > 0$ a.u. opens a new approach to characterize the CEP.

We now employ a classical model in order to explain and characterize the extension of the energy-resolved photoelectron spectra. According to the simple-man's model [53] the physical mechanism behind ATI process will be as follows: at a given time, that we call ionization time t_i, an atomic electron is released or born at the position $z = 0$ with zero velocity, i.e., $\dot{z}(t_i) = 0$. This electron now moves only under the influence of the oscillating laser electric field (this model neglects the Coulomb interaction with the remaining ion) and will reach the detector either directly or through the process known as rescattering. By using the classical equation of motion of an electron moving in an oscillating electric field, it is possible to calculate the maximum energy of the electron for both the direct and rescattered processes.
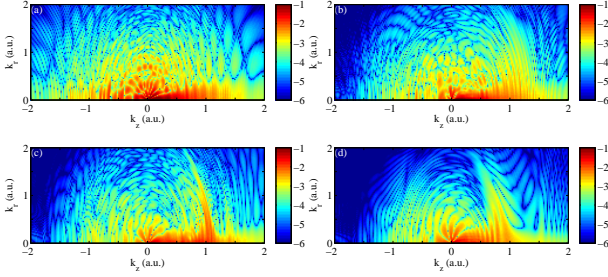

FIG. 11. (Color online) Idem Fig. 8 but for $\phi = 3\pi/2$

The Newton equation of motion for the atomic electron in the laser electric field can be written, using the functional form of Eq. (1), as follows

$$\ddot{z}(t) = -\nabla_z V_l(\mathbf{r}, t) \qquad (3)$$
$$= E(t)[1 + 2\beta z(t)] \qquad (4)$$

where we have collected the time-dependent part of the electric field in $E(t)$, i.e., $E(t) = E_0 f(t) \sin(\omega t + \phi)$.

In the limit where $\beta = 0$ in Eq. (3), we recover the homogeneous case. For the direct laser ionization, the kinetic energy of an electron released or born at time t_i is

$$E_k^d = \frac{[\dot{z}(t_i) - \dot{z}(t_f)]^2}{2}, \qquad (5)$$

where t_f is the end time of the laser pulse. For the rescattered laser-ionized electron, in which the electron returns to the core at a time t_r and reverses its direction, the kinetic energy of the electron yields

$$E_k^r = \frac{[\dot{z}(t_i) + \dot{z}(t_f) - 2\dot{z}(t_r)]^2}{2}. \qquad (6)$$

For homogeneous fields, Equations (5) and (6) become the usual expressions $E_k^d = \frac{[A(t_i) - A(t_f)]^2}{2}$ and $E_k^r = \frac{[A(t_i) + A(t_f) - 2A(t_r)]^2}{2}$, with $A(t)$ being the laser vector potential $A(t) = -\int^t E(t')dt'$, respectively. For the case
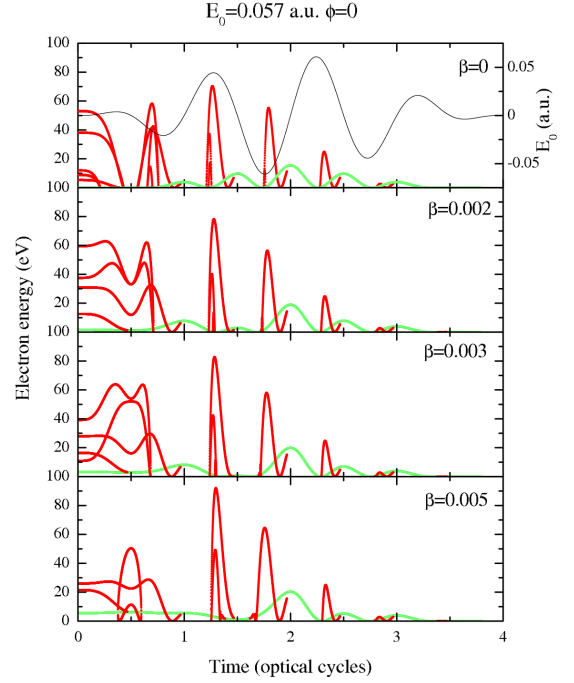

FIG. 12. (Color online) Numerical solutions of the Newton equation [Eq. (3)] plotted in terms of the direct and rescattered electron kinetic energy, E_k^d and E_k^r, respectively. The laser parameters are $I = 1.140 \times 10^{14}$ W/cm^2 ($E_0 = 0.057$ a.u), $\lambda = 800$ nm and $\phi = 0$. We employ a few-cycle laser pulse with 4 total cycles (10 fs). Different panels correspond to various values of β (see labels). Green filled circles: *direct* electrons; red filled circles: *rescattered* electrons.

with $\beta = 0$, it can be shown that the maximum value for E_k^d is $2U_p$ while for E_k^r it is $10U_p$ [1]. These two values appear as cutoffs in the energy resolved photoelectron spectrum as can be observed in panels (a) of Figs. 2 and 3.

In Figs. 12-19, we present the numerical solutions of Eq. (3), which is plotted in terms of the kinetic energy (in eV) of the direct and rescattered electrons.

Figures 12-15 are for a laser intensity of $I = 1.140 \times 10^{14}$ W/cm^2 ($E_0 = 0.057$ a.u.) meanwhile in Figs. 16-19 the laser intensity is $I = 5.404 \times 10^{14}$ W/cm^2 ($E_0 = 0.12$ a.u.). Figures 12 (16), 13 (17), 14 (18) and 15 (19) are for $\phi = 0$, $\phi = \pi/2$, $\phi = \pi$, $\phi = 3\pi/2$, respectively and for different values of the β parameter ($\beta = 0$ (homogeneous case), $\beta = 0.002$, $\beta = 0.003$ and $\beta = 0.005$, from top to bottom).

From the curves for $\beta \neq 0$ we can observe the strong modifications that the nonhomogeneous character of the laser electric field produces in the kinetic energy of the laser-ionized electron. Furthermore, it is possible to observe how the kinetic energy is more sensitive to the CEP. If we analyze, for instance, the top panels of Figs. 12-15 (i.e the homogeneous case) we conclude that the shape of both the kinetic energy of the direct and rescattered electron are identical for $\phi = 0$ ($\phi = \pi/2$) and $\phi = \pi$ ($\phi = 3\pi/2$). On the other hand, for the different values
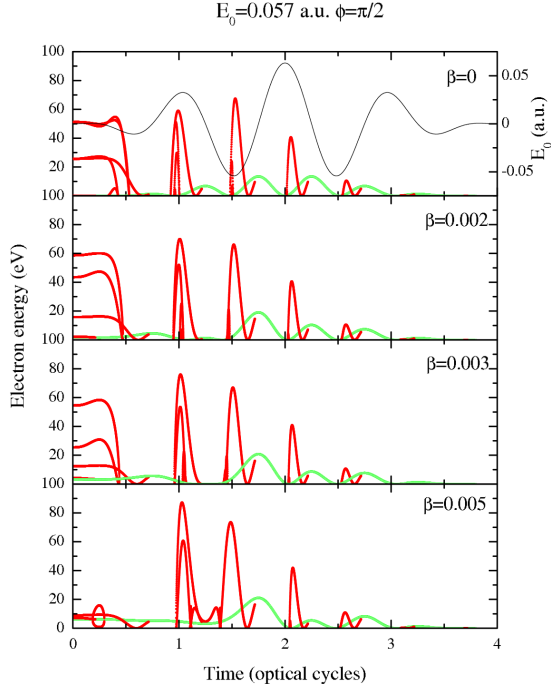
E_0=0.057 a.u. $\phi=\pi/2$

FIG. 13. (Color online) Idem Fig. 12 for $\phi = \pi/2$.

E_0=0.057 a.u. $\phi=\pi$

FIG. 14. (Color online) Idem Fig. 12 for $\phi = \pi$.

E_0=0.057 a.u. $\phi=3\pi/2$
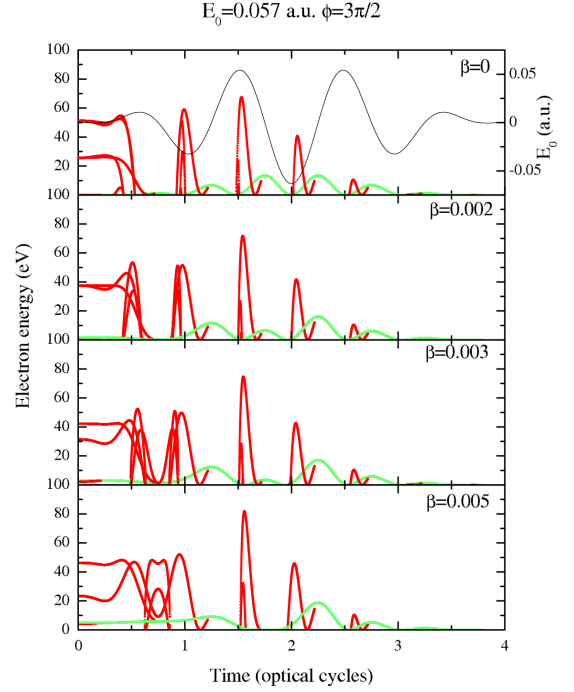
FIG. 15. (Color online) Idem Fig. 12 for $\phi = 3\pi/2$.

this way it spends more time in the continuum acquiring energy from the laser electric field. Consequently, higher values of the kinetic energy are attained. This distinct behavior is more evident for $E_0 = 0.12$ a.u. and $\beta = 0.005$, but it appears to some degree for all the studied cases.

A similar behavior was observed recently in above threshold photoemission (ATP) using metal nanotips. According to the model developed in Ref. [31] the strong localized fields modify the electron motion in such a way to allow sub-cycle dynamics.

In our approach, however, we include the full picture of the ATI phenomenon, namely both direct and rescattered electrons are considered (in Ref. [31] only direct electrons are taken into account) and consequently the characterization of the dynamics of the photoelectrons is more complex. Nevertheless, the higher kinetic energy of the rescattered electrons is a clear consequence of the strong modifications the laser electric field produces in the region where the electron dynamics takes place, as in the above mentioned case of ATP.

B.   Multiphoton regime

For the multiphoton case, we consider a few-cycle laser pulse with 6 complete optical cycles and $E_0 = 0.05$ a.u. ($I = 8.775 \times 10^{13}$ W/cm^2) and $\omega = 0.25$ a.u. ($\lambda = 182.5$ nm). In here, the Keldysh parameter is $\gamma = 5$, indicating the predominance of the multiphoton process [11]. We have computed the $P(E)$, two-dimensional electron distributions and the classical electron energies for all the set
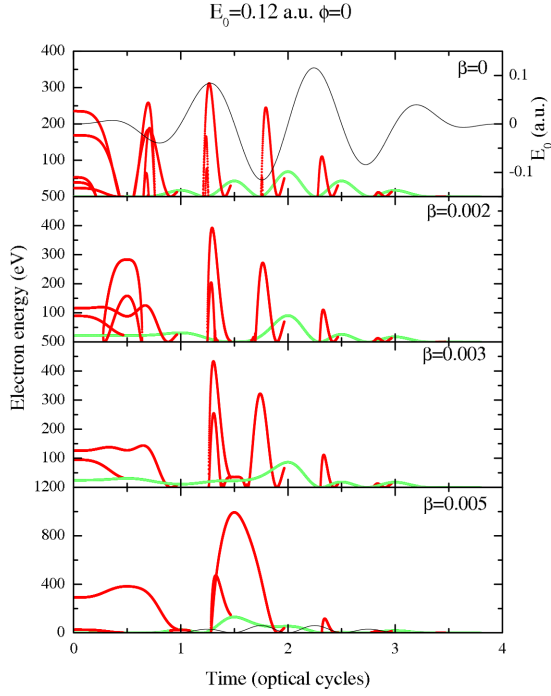
of β the kinetic energy has a unique shape for a given value of ϕ.

The particular features present for $\beta \neq 0$ are related to the changes in the laser-ionized electron trajectories (for details see e.g. [37–39]). In summary, the electron trajectories are modified in such a way that now the electron ionizes at an earlier time and recombines later, and in

$E_0=0.12$ a.u. $\phi=0$

FIG. 16. (Color online) Numerical solutions of the Newton equation [Eq. 3] plotted in terms of the direct and rescattered electron kinetic energy, E_k^d and E_k^r, respectively. The laser parameters are $I = 5.0544 \times 10^{14}$ W/cm^2 ($E_0 = 0.12$ a.u), $\lambda = 800$ nm and $\phi = 0$. We employ a few-cycle laser pulse with 4 total cycles (10 fs). Different panels correspond to various values of β (see labels). Green filled circles: *direct* electrons; red filled circles: *rescattered* electrons.

of cases presented in Sec. III.A. In this paper, however, we just present the most extreme case with an inhomogeneity factor of $\beta = 0.005$ and CEP of $\phi = \pi/2$. These results are presented in Figs. 20, 21 and 22 for $P(E)$, two-dimensional electron distributions and the classical electron energies, respectively. The $P(E)$ exhibits the usual multiphoton peaks [2, 48] and the inhomogeneity of the field does not play any significant role. In the whole range, the values of the yields have a difference of less than 5% and in a logarithmic scale this is hard to discern.

The two-dimensional electron distributions are also the same in terms of shape and magnitude for both homogeneous and inhomogeneous cases, as shown in Fig. 21. It means the differences introduced by the spatial nonhomogeneous character are practically imperceptible. We should note that our calculation is practically identical to the one presented in [11].

The numerical solutions of Eq. (3) as function of the kinetic energy (in eV) of the direct and rescattered electron is depicted in Fig. 22. In here, we could also observe, in support to our quantum mechanical calculations, that the inhomogeneity of the field does not change the electron energies in both the direct and rescattered processes.

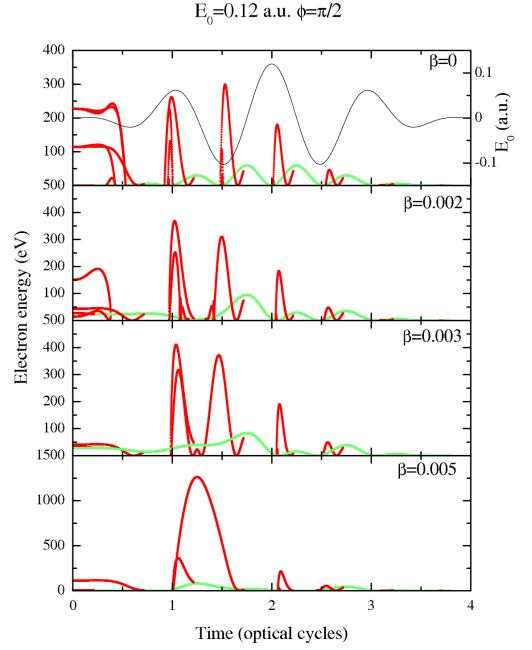In general, we do not find noticeable differences in

$E_0=0.12$ a.u. $\phi=\pi/2$

FIG. 17. (Color online) Idem Fig. 16 for $\phi = \pi/2$.
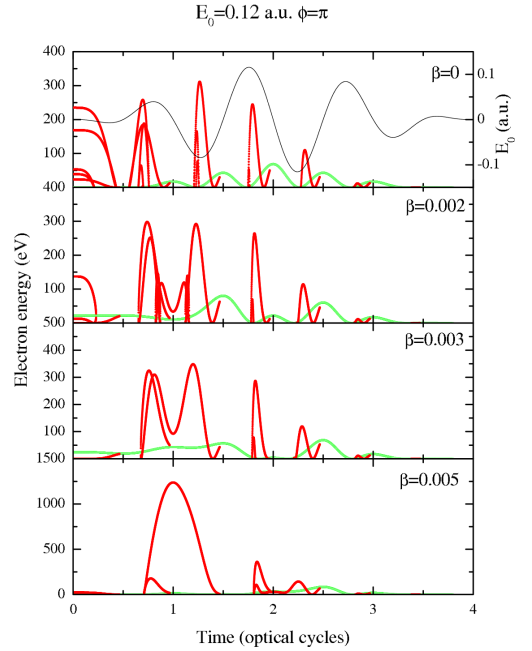

$E_0=0.12$ a.u. $\phi=\pi$

FIG. 18. (Color online) Idem Fig. 16 for $\phi = \pi$.

these observable quantities for both variations in the CEP and the strength of the inhomogeneity parameter β. As a result, we conclude that in the multiphoton regime the modifications introduced by the spatial inhomogeneities field do not produce appreciable modifications in the electron dynamics and consequently in the measurable quantities. In addition, the laser-ionized electron, in both the direct and rescattered processes, has a very small kinetic energy in the multiphoton regime due
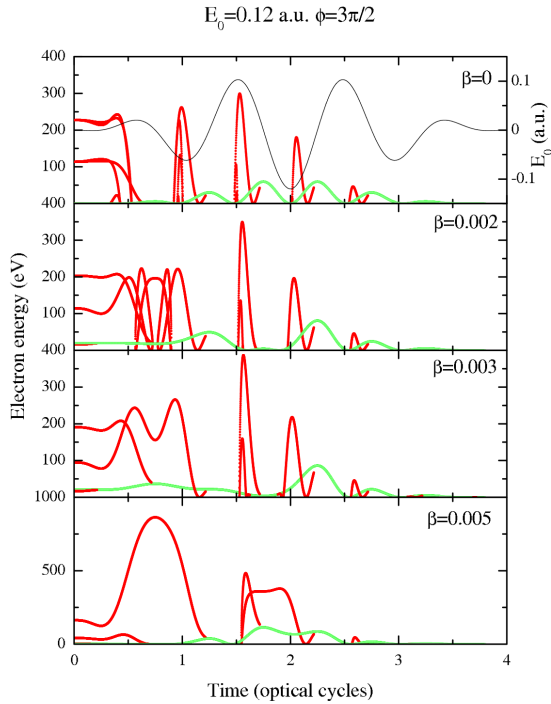
E$_0$=0.12 a.u. ϕ=3π/2

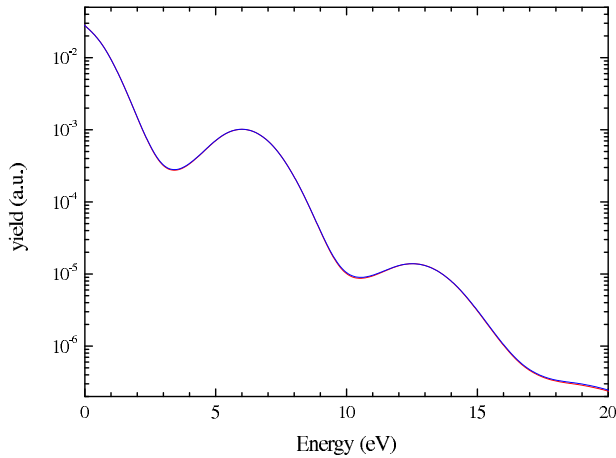FIG. 19. (Color online) Idem Fig. 16 for $\phi = 3\pi/2$.

FIG. 20. (Color online) Energy-resolved photoelectron spectra $P(E)$ calculated using the 3D-TDSE for an hydrogen atom ($I_p = -0.5$ a.u.). The laser parameters are $E_0 = 0.05$ a.u. ($I = 8.775 \times 10^{13}$ W/cm^2) and $\omega = 0.25$ a.u. ($\lambda = 182.5$ nm). We have used a sin-squared shaped pulse with a total duration of six optical cycles and $\phi = \pi/2$. Red line: homogeneous case ($\beta = 0$); blue line: $\beta = 0.005$;.

FIG. 21. (Color online) Two-dimensional electron momentum distributions (logarithmic scale) in cylindrical coordinates (k_z, k_r) using the exact 3D-TDSE calculation for an hydrogen atom. The laser parameters are $E_0 = 0.05$ a.u. ($I = 8.775 \times 10^{13}$ W/cm^2), $\omega = 0.25$ a.u. ($\lambda = 182.5$ nm) and $\phi = \pi/2$. We employ a laser pulse with 6 total cycles. Panel (a) corresponds to the homogeneous case ($\beta = 0$) and panel (b) is for $\beta = 0.005$.

IV. CONCLUSIONS AND OUTLOOK

We have extended our previous studies of ATI produced by nonhomogeneous fields using the three dimensional solutions of the TDSE. We have modified the 3D-TDSE to model the ATI phenomenon driven by spatial nonhomogeneous fields by including an additional term in the laser-atom coupling. In the tunneling regime we predict an extension in the cutoff position and an increase of the yield of the energy-resolved photoelectron spectra in certain regions. In addition, both the photoelectron spectra and the two-dimensional electron momentum distributions appear to be more sensitive to the carrier envelope phase of the laser electric field. This feature indicates that the ATI produced by spatial inhomogeneous field could be a good candidate for few-cycle laser pulse characterization. Furthermore, our predictions pave the way for the production of high-energy photoelectrons, reaching the keV regime, using plasmon enhanced fields. In the multiphoton regime, we show that both the $P(E)$ and the two-dimensional electron distributions are hardly affected by the spatial nonhomogeneities of the laser electric field. Our quantum mechanical calculations are supported by the classical simulations. In particular, the $P(E)$ characteristics are reasonably well reproduced by simulations based on classical physics.

to low intensity field. Indeed, in this case the maximum energy after the rescattering process has taken place is ≈ 3 eV. As a result, it is reasonable to have a very small or almost no differences between the final kinetic energies, when a spatial inhomogeneity of small strength is present.
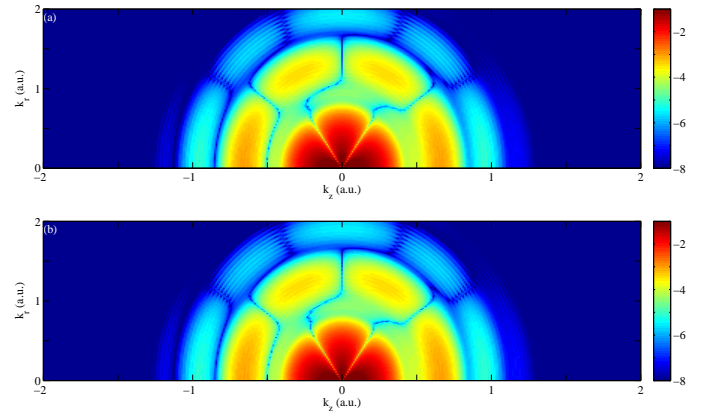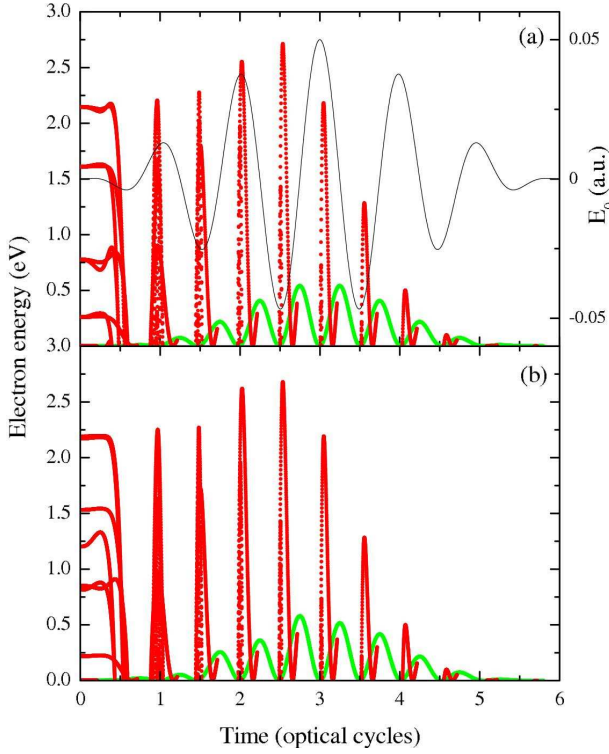
FIG. 22. (Color online) Numerical solutions of the Newton equation [Eq. (3)] plotted in terms of the direct and rescattered electron kinetic energy, E_k^d and E_k^r, respectively. The laser parameters are $E_0 = 0.05$ a.u. ($I = 8.775 \times 10^{13}$ W/cm^2), $\omega = 0.25$ a.u. ($\lambda = 182.5$ nm) and $\phi = \pi/2$. We employ a laser pulse with 6 total cycles. Panel (a) corresponds to the homogeneous case ($\beta = 0$) and panel (b) is for $\beta = 0.005$. Green filled circles: *direct* electrons; red filled circles: *rescattered* electrons.

[1] D. B. Milošević, G. G. Paulus, D. Bauer, and W. Becker, J. Phys. B **39**, R203 (2006).

[2] P. Agostini, F. Fabre, G. Mainfray, G. Petite, and N. K. Rahman, Phys. Rev. Lett. **42**, 1127 (1979).

[3] M. Schnürer, C. Streli, P. Wobrauschek, M. Hentschel, R. Kienberger, C. Spielmann, and F. Krausz, Phys. Rev. Lett. **85**, 3392 (2000).

[4] P. von den Hoff, I. Znakovskaya, M. Kling, and R. de Vivie-Riedle, Chem. Phys. **366**, 139 (2009).

[5] F. Ferrari, F. Calegari, M. Lucchini, C. Vozzi, S. Stagira, G. Sansone, and M. Nisoli, Nat. Phot. **4**, 975 (2010).

[6] M. Schultze, E. Goulielmakis, M. Uiberacker, M. Hofstetter, J. Kim, D. Kim, F. Krausz, and U. Kleineberg, N. Jour. of Phys. **9**, 243 (2007).

[7] J. Ullrich, R. Moshammer, R. Dörner, O. Jagutzki, V. Mergel, H. Schmidt-Böcking, and L. Spielberger, J. Phys. B **30**, 2917 (1997).

[8] A. Rudenko, K. Zrost, C. D. Schröter, V. L. B. de Jesus, B. Feuerstein, R. Moshammer, and J. Ullrich, J. Phys. B **37**, L407 (2004).

[9] C. M. Maharjan, A. S. Alnaser, I. Litvinyuk, P. Ranitovic, and C. L. Cocke, J. Phys. B **39**, 1955 (2006).

[10] M. Schuricke, G. Zhu, J. Steinmann, K. Simeonidis, I. Ivanov, A. Kheifets, A. N. Grum-Grzhimailo, K. Bartschat, A. Dorn, and J. Ullrich, Phys. Rev. A **83**, 023413 (2011).

[11] D. G. Arbó, J. E. Miraglia, M. S. Gravielle, K. Schiessl, E. Persson, and J. Burgdörfer, Phys. Rev. A **77**, 013401 (2008).

[12] T. Wittmann, B. Horvath, W. Helml, M. G. Schätzel, X. Gu, A. L. Cavalieri, G. G. Paulus, and R. Kienberger, Nat. Phys. **5**, 357 (2009).

[13] M. F. Kling, J. Rauschenberger, A. J. Verhoef, D. B. M. E. Hasović, T. Uphues, H. G. Muller, and M. J. J. Vrakking, New J. Phys. **10**, 025024 (2008).

[14] M. Nisoli, G. Sansone, S. Stagira, S. D. Silvestri, C. Vozzi, M. Pascolini, L. Poletto, P. Villoresi, and G. Tondello, Phys. Rev. Lett. **91**, 213905 (2003).

[15] G. G. Paulus, F. Grasbon, H. Walther, P. Villoresi, M. Nisoli, S. Stagira, E. Priori, and S. D. Silvestri, Nature **414**, 182 (2001).

[16] X. Liu, H. Rottke, E. Eremina, W. Sandner, E. Goulielmakis, K. O. Keeffe, M. Lezius, F. Krausz, F. Lindner, M. G. Schätzel, et al., Phys. Rev. Lett. **93**, 263001 (2004).

[17] A. M. Sayler, T. Rathje, M. Moller, D. Hoff, G. Stibenz, W. Müller, C. Kurbis, K. Rühle, and G. G. Paulus, (CLEO EUROPE/EQEC) p. 1 (2011).

[18] A. M. Sayler, T. Rathje, W. Müller, K. Rühle, R. Kienberger, and G. G. Paulus, Opt. Lett. **36**, 1 (2011).

[19] G. G. Paulus and et al., Nature **414**, 182 (2001).

[20] G. G. Paulus, F. Lindner, H. Walther, A. Baltuška, E. Goulielmakis, M. Lezius, and F. Krausz, Phys. Rev. Lett. **91**, 253004 (2003).

[21] S. Kim, J. Jin, Y.-J. Kim, I.-Y. Park, Y. Kim, and S.-W. Kim, Nature **453**, 757 (2008).

[22] I.-Y. Park, S. Kim, J. Choi, D.-H. L. Y.-J. Kim, M. F. Kling, M. I. Stockman, and S.-W. Kim, Nat. Phot. **5**, 677 (2011).

[23] M. Sivis, M. Duwe, B. Abel, and C. Ropers, Nature **485**, E1 (2012).

[24] S. Kim, J. Jin, Y.-J. Kim, I.-Y. Park, Y. Kim, and S.-W. Kim, Nature **485**, E2 (2012).

[25] S. Zherebtsov and et. al, Nat. Physics **7**, 656 (2011).

[26] M. Krüger, M. Schenk, and P. Hommelhoff, Nature **475**, 78 (2011).

[27] P. Hommelhoff, Y. Sortais, A. Aghajani-Talesh, and M. A. Kasevich, Phys. Rev. Lett. **96**, 077401 (2006).

[28] M. Schenk, M. Krüger, and P. Hommelhoff, Phys. Rev. Lett. **105**, 257601 (2010).

[29] M. Krüger, M. Schenk, M. Förster, and P. Hommelhoff, J. Phys. B **45**, 074006 (2012).

[30] P. Dombi, P. Racz, J. Fekete, A. Thai, S. Teichmann, O. Chalus, P. K. Bates, and J. Biegert, Lasers and Electro-Optics (CLEO), 2011 Conference on pp. 1–2 (2011).

[31] G. Herink, D. R. Solli, M. Gulde, and C. Ropers, Nature **483**, 190 (2012).

[32] A. Apolonski and et al., Phys. Rev. Lett. **92**, 073902 (2004).

[33] P. Dombi, P. Racz, and B. Bodi, Laser Part. Beams **27**, 291 (2009).

[34] M. Protopapas, C. H. Keitel, and P. L. Knight, Rep. Prog. Phys. **60**, 389 (1997).

[35] T. Brabec and F. Krausz, Rev. Mod. Phys. **72**, 545 (2000).

[36] A. Husakou, S.-J. Im, and J. Herrmann, Phys. Rev. A **83**, 043839 (2011).

[37] M. F. Ciappina, J. Biegert, R. Quidant, and M. Lewenstein, Phys. Rev. A **85**, 033828 (2012).

[38] I. Yavuz, E. A. Bleda, Z. Altun, and T. Topcu, Phys. Rev. A **85**, 013416 (2012).

[39] M. F. Ciappina, S. S. Aćimović, T. Shaaran, J. Biegert, R. Quidant, and M. Lewenstein, Opt. Exp. **20**, 26261 (2012).

[40] M. F. Ciappina, J. A. Pérez-Hernández, T. Shaaran, J. Biegert, R. Quidant, and M. Lewenstein, Phys. Rev. A **86**, 023413 (2012).

[41] T. Shaaran, M. F. Ciappina, and M. Lewenstein, Phys. Rev. A **86**, 023408 (2012).

[42] T. Shaaran, M. F. Ciappina, and M. Lewenstein, J. Mod. Opt. **59**, 1634 (2012).

[43] K. J. Schafer, Y. Baouri, L. F. DiMauro, and K. C. Kulander, Phys. Rev. Lett. **70**, 1599 (1993).

[44] D. A. Telnov and S. Chu, Phys. Rev. A **79**, 043421 (2009).

[45] D. Bauer and P. Koval, Comp. Phys. Comm. **174**, 396 (2006).

[46] C. I. Blaga, F. Catoire, P. Colosimo, G. G. Paulus, H. G. Muller, P. Agostini, and L. F. DiMauro, Nat. Phys. **5**, 335 (2009).

[47] W. Quan, Z. Lin, M. Wu, H. Kang, H. Liu, X. Liu, J. Chen, J. Liu, X. T. He, S. G. Chen, et al., Phys. Rev. Lett. **103**, 093001 (2009).

[48] K. J. Schafer and K. C. Kulander, Phys. Rev. A **42**, 5794 (1990).

[49] K. J. Schafer, Comp. Phys. Comm. **63**, 427 (1991).

[50] K. J. Schafer, *Numerical Methods in Strong Field Physics, in Strong Field Laser Physics, ed. T. Brabec Springer Series in Optical Sciences* (Springer, Berlin, 2008).

[51] H. R. Reiss, Phys. Rev. A **75**, 031404(R) (2007).

[52] H. R. Reiss, Phys. Rev. A **82**, 023418 (2010).

[53] P. B. Corkum, Phys. Rev. Lett **71**, 1994 (1993).